EPJ Photovoltaics **11**, 4 (2020)

https://doi.org/10.1051/epjpv/2020002

Available online at:
www.epj-pv.org

REGULAR ARTICLE OPEN ACCESS

Electrical characterization of low temperature plasma epitaxial Si grown on highly doped Si substrates

Cyril Leon[1,2,3,*], Sylvain Le Gall[1,2,3], Marie-Estelle Gueunier-Farret[1,2,3], Jean-Paul Kleider[1,2,3], and Pere Roca i Cabarrocas[3,4]

[1] Université Paris-Saclay, CentraleSupélec, CNRS, Laboratoire de Génie Electrique et Electronique de Paris, 91192 Gif-sur-Yvette, France
[2] Sorbonne Université, CNRS, Laboratoire de Génie Electrique et Electronique de Paris, 75252 Paris, France
[3] Institut Photovoltaïque d'Ile-de-France (IPVF), 30 Route départementale 128, 91120 Palaiseau, France
[4] LPICM, CNRS, Ecole polytechnique, IP Paris, 91128 Palaiseau, France

Received: 8 October 2019 / Received in final form: 19 December 2019 / Accepted: 7 January 2020

Abstract. Epitaxial silicon layers were grown on highly doped c-Si substrates using the plasma-enhanced chemical vapour deposition process (PECVD) at low temperature (175 °C). The transport and defect-related properties of these epi-Si layers were characterized by current density-voltage (J–V) and capacitance–voltage (C–V) techniques. The results show that the epi-Si layers exhibit a non-intentional n-type doping with a low apparent doping density of about 2×10^{15} cm^{-3}. The admittance spectroscopy technique is used to investigate the presence of deep-level defects in the structure. An energy level at 0.2 eV below the conduction band has been found with a density in the range of 10^{15} cm^{-3} which may explain the observed apparent doping profile.

Keywords: Capacitance–voltage / current–voltage / impurity profile / epitaxial Si

1 Introduction

Low temperature plasma epitaxy has been developed over the past years. The process, based on the interaction of positively charged clusters with the film surface has been studied experimentally [1,2] and modeled using ab initio simulations [3]. Moreover, thin epitaxial layers have been successfully integrated into heterojunction type solar cells on cristalline silicon (c-Si) wafers [4,5] and successfully transferred to glass substrates [6,7] resulting in devices with energy conversion efficiencies in the range of 6–8%. Modeling the J–V characteristics and external quantum efficiency of such devices has revealed that the defect density in these epitaxial layers should be around 1×10^{15} cm^{-3} and that efficiencies up to 13% are within reach [8]. In this paper we use current density-voltage (J–V) and capacitance–voltage (C–V) measurements to study the electrical properties (transport and defect states) of Schottky diodes made with a thin crystalline silicon film grown using epitaxy at 175 °C on a highly doped c-Si substrate.

2 Fabrication process

Undoped (non-intentionally doped) hydrogenated crystalline silicon layers (epi-Si) were deposited by plasma-enhanced chemical vapour deposition (PECVD) at 175 °C from the dissociation of silane-hydrogen mixtures in a hot-wall multi-plasma monochamber reactor [9]. The films were co-deposited on highly doped p^{++} and n^{++} (100) oriented crystalline silicon substrates with resistivity values below 0.005 ohm.cm and cleaned either using a standard dip in a 5% HF solution for 30 s or in-situ in the plasma reactor using an SiF_4 plasma [10]. In the following, the structures will be denoted "$(epi/p^{++})_i$" and "$(epi/n^{++})_i$" for the epi-Si deposited on p^{++} and n^{++} c-Si substrates, respectively (with i the sample number). After deposition the films were characterized by spectroscopic ellipsometry measurements from which their crystallinity and their thickness were determined. Au contacts were thermally evaporated through a shadow mask to define the area of the devices (1 mm and 2 mm diameter dots). Al contact was deposited on the rear side of the structure. Measurements were performed between the Au and the Al contacts. Table 1 summarizes the growth conditions for the samples presented in this study.

3 Current–voltage measurements

The dark J–V characteristics are shown in Figure 2 for both $(epi/p^{++})_i$ (Fig. 2a) and $(epi/n^{++})_i$ (Fig. 2b). It can be observed that the $(epi/n^{++})_i$ exhibit a single junction behavior with one barrier at one electrode and no barrier at the other one, while the linear current for both polarities in

* e-mail: cyril.leon@geeps.centralesupelec.fr

Table 1. PECVD growth conditions on both n^{++} and p^{++} substrates. The substrate temperature and RF power were fixed at 175 °C and 10 Watts, respectively. The H_2 and SiH_4 fluxes were set at 350 sccm and 5 sccm, respectively. Di refers to the inter-electrode distance in the PECVD reactor.

Sample	Thickness (μm)	Di (mm)	Pressure (mTorr)
1	1.5	22	1950
2	1.14	22	1823
3	1.1	12	2300
4	1.3	12	2300

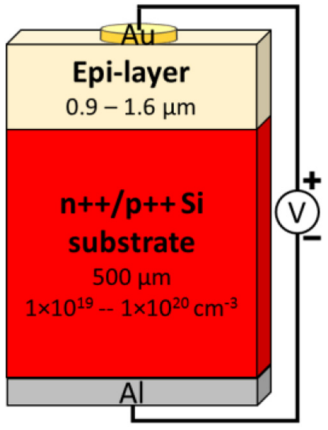

Fig. 1. Sketch of the structure.

the $(epi/p^{++})_i$ suggests a more symmetrical band diagram. The difference of J–V curves behavior between the measurements performed on the $(epi/n^{++})_i$ and the $(epi/p^{++})_i$ can be explained if we consider that the epitaxial silicon layer is of n-type. Actually, n-type epi-layer on a p^{++} substrate with Au contact (considering a work function of 4.85 eV [11]) leads to two barriers on both sides of the epitaxial layer as shown in the band diagram of the structure in Figure 3a. On the other hand, considering the $(epi/n^{++})_i$, the structure is the one of a front Schottky diode with an ohmic back contact as sketched by the band diagram in Figure 3b. Thus, in the following, further characterization techniques will be performed on the $(epi/n^{++})_i$.

4 Capacitance–voltage measurements

C–V measurements are used to probe the space charge region (SCR) of the epi-Si layers deposited on n^{++} substrates. The capacitance is measured with an LCR-meter that provides a small AC voltage signal of 20 mV. At high frequency range (around 100 kHz), the capacitive effect is only driven by the depletion capacitance: the variation of the width of the depletion zone with the applied voltage induces a depletion capacitance which predominates in reverse bias. The depletion capacitance C per unit area in a Schottky diode is given by [12]:

$$C = \frac{\varepsilon}{w} = \sqrt{\frac{\varepsilon q N_{CV}}{2\left(\psi_0 - V - \frac{k_B T}{q}\right)}}, \quad (1)$$

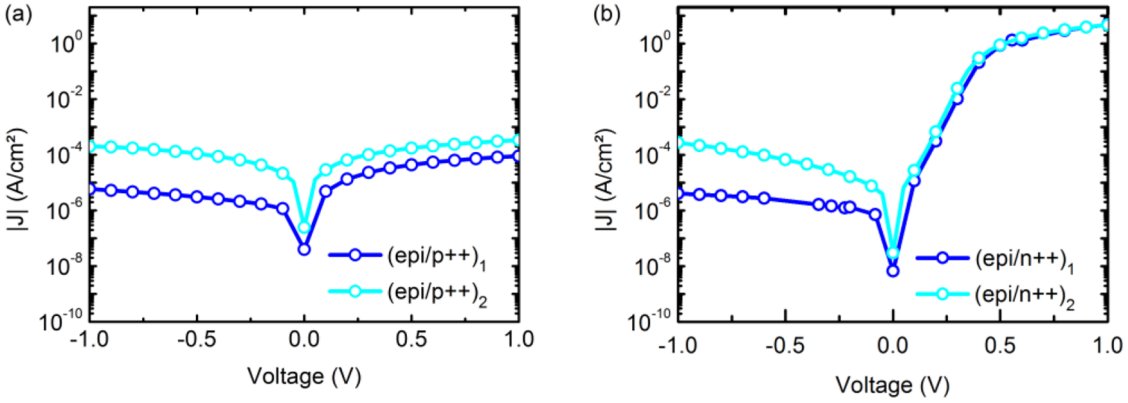

Fig. 2. Dark J–V characteristics obtained at room temperature on (a) $(epi/p^{++})_i$ and (b) $(epi/n^{++})_i$.

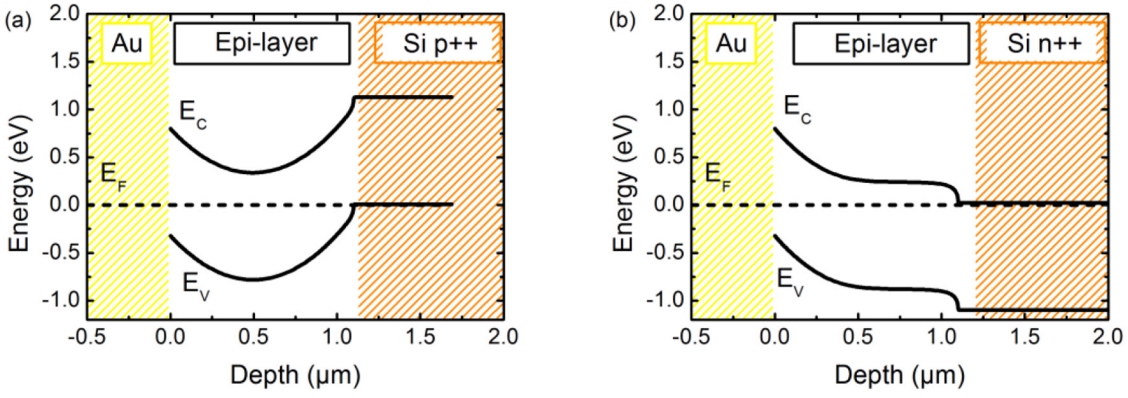

Fig. 3. Sketches of the band diagram of (a) the $(epi/p^{++})_i$ and (b) the $(epi/n^{++})_i$.

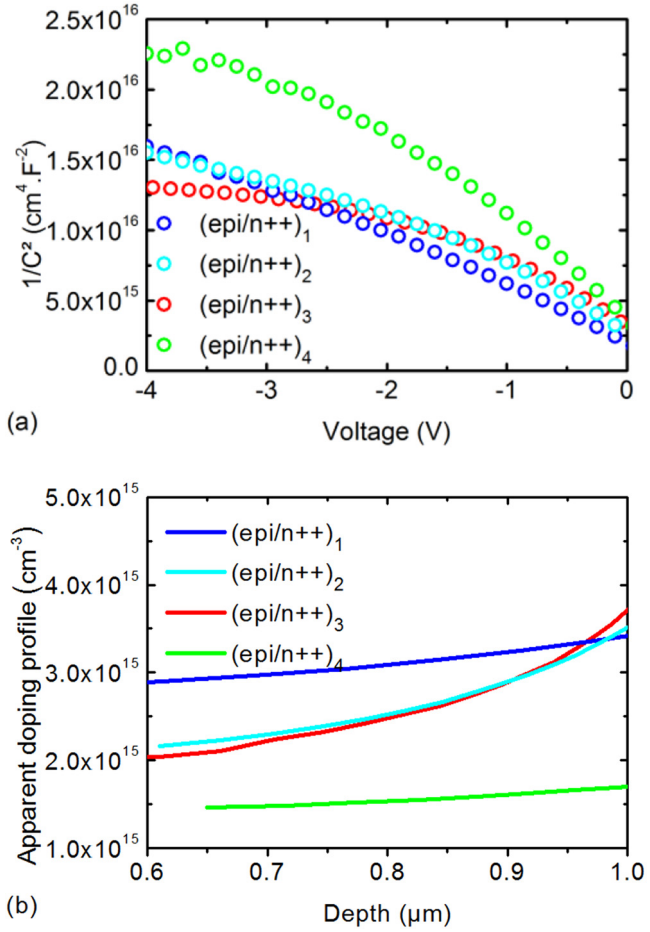

Fig. 4. (a) Mott-Schottky plots of the $(\text{epi/n}^{++})_{\text{i}}$ structure and (b) the apparent doping profiles extracted from the slopes of the Mott-Schottky plots (Eq. (2)).

where q is the elementary charge, ψ_0 the equilibrium built-in potential of the SCR, ε the dielectric permittivity, N_{CV} the apparent doping density ($N_{CV} = N_D$ if we consider the epi-Si as n-type), k_{B} the Boltzmann constant, V the applied voltage, T the temperature and w the width of the SCR. The Mott-Schottky plot, i.e. the plot of $1/C^2$ versus the reverse applied voltage, yields a straight line with a slope related to N_{CV}:

$$\frac{d(1/C^2)}{dV} = \frac{-2}{q\varepsilon N_{CV}}. \tag{2}$$

This can be extended to non-uniform doping in order to obtain a doping profile, the slope at bias V being related to the doping density at the edge w of the SCR, calculated from $w = \varepsilon/C$ [12].

C–V measurements performed on the $(\text{epi/n}^{++})_{\text{i}}$ structures reveal a non-linear Mott-Schottky plot as shown in Figure 4a. The apparent doping densities N_{CV} extracted from the slopes (Eq. (2)) in the quasi-linear region (between −1 and 0 V) are represented as a function of the depth from the Schottky contact in Figure 4b. We can observe that they are in the range of 10^{15} cm^{-3}. With this low doping densities, as expected, the width of the space charge region is in the micron range and thus in the range of the thickness of the epi-layer (e). Since the width of the depletion zone cannot be thicker than the thickness of the epi-layer, for high reverse voltage bias, the Mott-Schottky plot tends toward $(e/\varepsilon)^2$. The slopes of the Mott-Schottky plots being impacted by this limit, it is not relevant to extract the doping densities for such voltage range. However, in the quasi-linear region, the slopes give a good idea of the apparent doping profile in the structure.

Because there is no intentional doping in the structure, the measured apparent doping profiles may come from the presence of impurities causing shallow and/or deep-level defects in the gap of the epitaxial layer. It is well known that such defects should even be more visible in the dependence upon temperature and frequency of the capacitance, e.g. in the capacitance spectroscopy technique. Thus, in the next section, we present capacitance spectroscopy measurements performed on the $(\text{epi/n}^{++})_{\text{i}}$.

5 Admittance spectroscopy

If deep-level defects (electrically active) are present in the gap of semiconductors they can contribute to the measured capacitance at low frequency. If the frequency of the AC signal is high enough compared to the inverse of the characteristic time of carrier exchange between the defect and the majority carrier band, then this contribution tends to vanish. It results in a step in the capacitance–frequency curve (C-f). The frequency of the inflexion point for an electron trap is described as follows [13]:

$$f_0 = \frac{\sigma_n \nu_{th} N_C}{\pi} e^{\frac{-E_a}{k_B T}} \tag{3}$$

where σ_n is the capture cross section for the electrons, ν_{th} is the thermal velocity of the electrons, N_c is the effective density of electrons in the conduction band, and E_a is the activation energy of the deep-level defect (energy position in the gap with respect to the conduction band).

Figure 5 presents C–f–T measurements at 0 V for $(\text{epi/n}^{++})_4$ (Fig. 5a) and $(\text{epi/n}^{++})_1$ (Fig. 5b). Almost no frequency dependence is observed for $(\text{epi/n}^{++})_4$ such that no information on active defects in the gap can be obtained. For $(\text{epi/n}^{++})_1$, a step in the C-f curves is observed and the frequency position of the inflexion point f_0 increases when the temperature increases. By extracting f_0 for various temperatures and by representing those values in an Arrhenius plot (Fig. 6), we observe a straight line with a slope being related to the activation energy of the deep-level defect. For $(\text{epi/n}^{++})_1$, the activation energy E_a is found equal to 0.20 eV.

We further investigated the influence of the deep-level defects on the curvature of the Mott-Schottky plots. The C–V curve of the $(\text{epi/n}^{++})_1$ at 300 K is measured for two frequencies of the AC signal: 200 Hz and 200 kHz. Those frequencies are chosen based on Figure 5b: at 200 Hz the defects should contribute to the total capacitance while at 200 kHz this contribution should be minimized. Mott-Schottky plots for both frequencies are compared in Figure 7. Apparent doping density values, N_{CV}, are

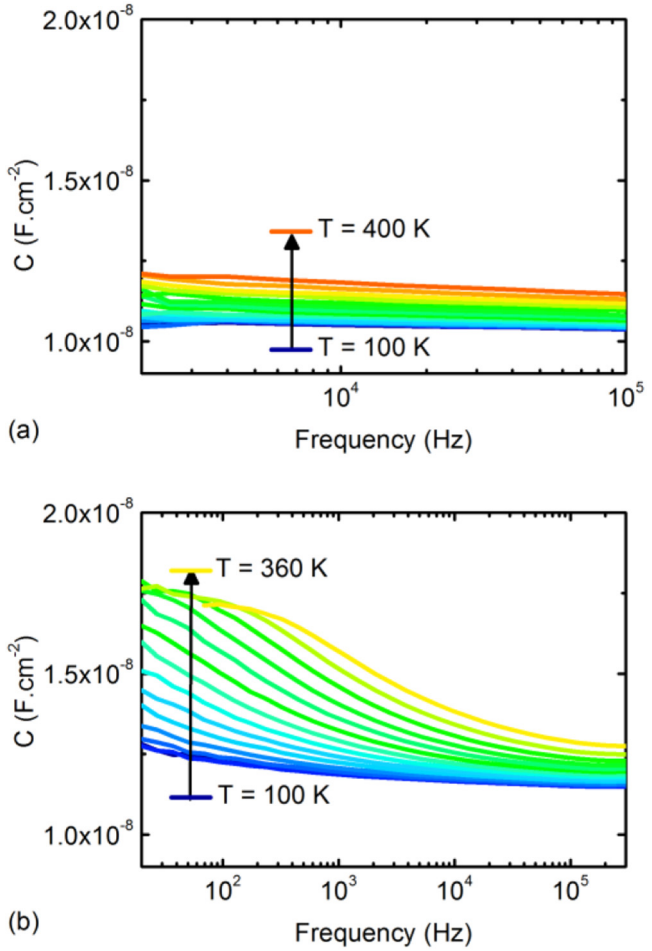

Fig. 5. C–f plots at 0 V for several temperatures for (a) $(\text{epi/n}^{++})_4$ and (b) $(\text{epi/n}^{++})_1$.

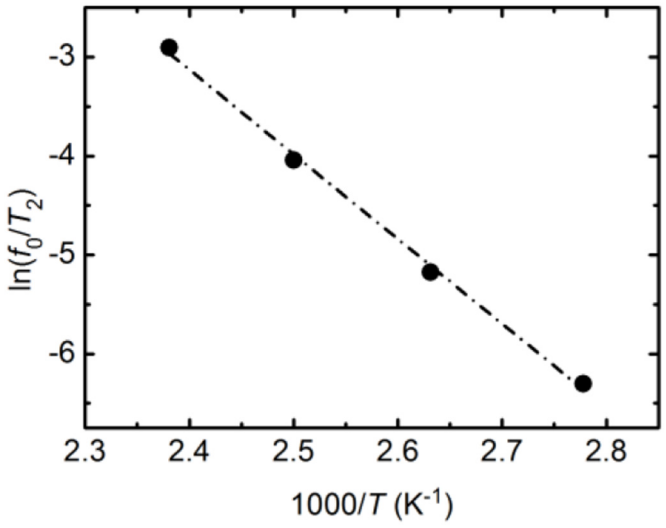

Fig. 6. Arrhenius plot of the frequency vs. $1000/T$ of the C–f inflexion points for $(\text{epi/n}^{++})_1$ (black dots). The dash-dotted line represents the linear fit used to deduce the activation energy (0.2 eV).

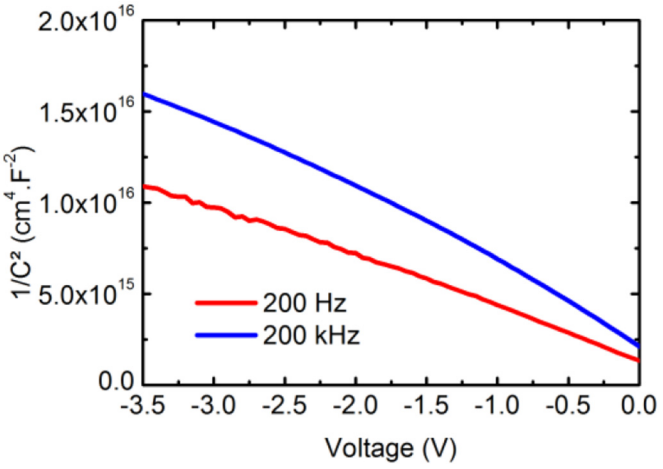

Fig. 7. Mott-Schottky plots of the $(\text{epi/n}^{++})_1$ measured at 300 K using two different frequency values of the AC signal to highlight the influence of the defects on the curvature of the $1/C^2(V)$ curve.

extracted for both curves at low reverse voltage, where the capacitance values are assumed to be not limited by the thickness of the epi-layer. We obtain N_{CV} values of 2.8×10^{15} cm^{-3} and 1.7×10^{15} cm^{-3} at 200 Hz and 200 kHz, respectively. The decrease of N_{CV} when the frequency is increased is in agreement with our assumption that the non-intentional doping of the epi-layer results from defects in the bandgap. However, the small difference between the extracted apparent doping densities corresponding to the two selected frequencies suggests that the defect density in this sample is low, in the range of 10^{15} cm^{-3}.

6 Conclusion

We demonstrated the presence of a low apparent n-type doping density in the range of 10^{15} cm^{-3} in unintentionally doped epitaxial silicon layers grown using low temperature PECVD. The frequency dependence of the C–V and Mott-Schottky plots indicates that deep-level defects with concentration in the same range of 10^{15} cm^{-3} do contribute to the apparent doping. Such defects were also observed in capacitance spectroscopy. However, the use of capacitance techniques to characterize the doping and defects densities was limited by the small thickness of the available samples, of the order of one micron, that is in the same range as the depletion region formed at the front Au Schottky barrier. A study performed on thicker samples is thus needed for more refined quantitative extractions and to understand the origin of the shallow and deep-level defects in this material.

Author contribution statement

All authors contributed equally to this study.

References

1. P. Roca i Cabarrocas, K.-H. Kim, R. Cariou, M. Labrune, E.V. Johnson, M. Moreno, A.T. Rios, S. Abolmasov, S. Kasouit, Low temperature plasma synthesis of nanocrystals

and their application to the growth of crystalline silicon and germanium thin films, Mat. Res. Soc. Symp. Proc. **1426**, 319 (2012)
2. W. Chen, G. Hamon, R. Leal, J.-L. Maurice, L. Largeau, P. Roca i Cabarrocas, Growth of tetragonal Si via plasma-enhanced epitaxy, Cryst. Growth Des. **17**, 8 (2017)
3. H. Le, F. Jardali, H. Vach, Deposition of hydrogenated silicon clusters for efficient epitaxial growth, Phys. Chem. Chem. Phys. **20**, 15626 (2018)
4. R. Cariou, M. Labrune, P. Roca i Cabarrocas, Thin crystalline silicon solar cells based on epitaxial films grown at 165 °C by RF PECVD, Solar Energy Mater. Sol. Cells **95**, 2260 (2011)
5. R. Cariou, J. Tang, N. Ramay, R. Ruggeri, P. Roca i Cabarrocas, Low temperature epitaxial growth of SiGe absorber for thin film heterojunction solar cells, Sol. Energy Mater. Sol. Cells **134**, 15 (2015)
6. W. Chen, R. Cariou, M. Foldyna, V. Depauw, C. Trompoukis, E. Drouard, L. Lalouat, A. Harouri, J. Liu, A. Fave, R. Orobtchouk, F. Mandorlo, C. Seassal, I. Massiot, A. Dmitriev, K.-D. Lee, P. Roca i Cabarrocas, Nano-photonics-based low temperature PECVD epitaxial crystalline silicon solar cells, J. Phys. D Appl. Phys. **49**, 12 (2016)
7. R. Cariou, W. Chen, I. Cosme-Bolanos, J.-L. Maurice, M. Foldyna, V. Depauw, G. Patriarche, A. Gaucher, A. Cattoni, I. Massiot, S. Collin, E. Cadel, P. Pareige, P. Roca i Cabarrocas, Ultra-thin PECVD epitaxial Si solar cells on glass via low temperature transfer process, Prog. Photovolt. Res. Appl. **24**, 1075 (2016)
8. S. Chakraborty, R. Cariou, M. Labrune, P. Roca i Cabarrocas, P. Chatterjee, Feasibility of using thin crystalline silicon films epitaxially grown at 165 °C in solar cells: A computer simulation study, EPJ Photovoltaics **4**, 45103 (2013)
9. P. Roca i Cabarrocas, J.B. Chévrier, J. Huc, A. Lloret, J.Y. Parey, J.P.M. Schmitt, A fully automated hot-wall multiplasma-monochamber reactor for thin film deposition, J. Vac. Sci. Technol. **9**, 2331 (1991)
10. M. Moreno, P. Roca i Cabaroccas, Ultra-thin crystalline silicon films produced by plasma assisted epitaxial growth on silicon wafers and their transfer to foreign substrates, EPJ Photovoltaics **1**, 10301 (2010)
11. S.M. Sze, *Physics of Semiconductor Devices*, 2nd edn. (John Wiley & Sons, New Jersey, 1981)
12. E.H. Rhoderick, Metal-semiconductor contacts, IEEE Proc. I Solid State Electron Dev. **129**, 1 (1982)
13. D.L. Losee. Admittance spectroscopy of impurity levels in Schottky barriers, J. Appl. Phys. **46**, 5 (1975)

Cite this article as: Cyril Leon, Sylvain Le Gall, Marie-Estelle Gueunier-Farret, Jean-Paul Kleider, Pere Roca i Cabarrocas, Electrical characterization of low temperature plasma epitaxial Si grown on highly doped Si substrates, EPJ Photovoltaics **11**, 4 (2020)